Energy Conversion and Management 268 (2022) 116003

Contents lists available at ScienceDirect

Energy Conversion and Management

journal homepage: www.elsevier.com/locate/enconman

Assessment of experimental 1D and analytical 3D steady approaches of packed bed thermal conversion through the simulation of a 60-kW biomass boiler operating at half and full load

B. Rajh [a,b], M.A. Gómez [c,*], C. Álvarez-Bermúdez [c], N. Cid [c], J.L. Míguez [c]

[a] Faculty of Mechanical Engineering, University of Maribor, Smetanova 17, 2000 Maribor, Slovenia
[b] Institute for Environmental Protection and Sensors, Beloruska 7, 2000 Maribor, Slovenia
[c] CINTECX, Grupo de Tecnología Energética (GTE), Universidade de Vigo, Lagoas-Marcosende s/n 36310, Vigo, Spain

ARTICLE INFO

Keywords:
Biomass
Combustion
Cfd simulation
Thermal conversion
Char oxidation

ABSTRACT

Among the different modelling strategies applied for the simulation of packed bed biomass combustion during the last two decades, the present paper detailed describes two models based on two of the most commonly used approaches and tests their performance through the simulation of a 60-kW wood pellet boiler. This contributes to analyze the behavior of both approaches working in different operating conditions and to determine what conditions are favorable for the models application. The first presented model is a 1D experimental method that introduces the products of the biomass thermal conversion through several sections of the bed top surface. The calculations are based on mass and energy balances and experimental determination of the reactive fluxes. The second model is an analytical 3D method that calculates the packed bed thermal conversion inside the CFD domain. This applies more complex calculations with a higher computational cost. For both models, the char oxidation reaction is calculated though four correlations that returns different CO/CO_2 ratios. The bed conversion models and the char oxidation correlations are applied to two different tests with the boiler operating at half and full load with different fuels. The results show that both bed models have a similar overall behaviour. The 3D model has a reasonably good behaviour in all cases and is not significantly affected by the different char correlations. Both models give similar results when combustion conditions are favourable (full-load test). The 1D model is highly sensitive to the char oxidation correlations, especially in the half load test. In this case, it has a better behaviour with the correlations that produce lower CO/CO_2 ratios. The analysis of the contours in the freeboard shows that, in the 3D bed model, an important part of the combustion process occurs in the bed volume, which is not meshed in the 1D model, and that advance in the combustion compensates the differences in the CO emitted by the bed.

1. Introduction

The EU has set the long-term goal to develop a low carbon economy by 2050 where bioeconomy will play an important role [1,2]. Solid biomass (e.g., wood pellets, chips and wood logs) will be one of the key fuels in future for the global energy transition [3]. Bioenergy can contribute substantially to reaching EU goals for successful green transition [4] and sufficient greenhouse gas emission reduction [5]. During the last 30 years, small-scale wood biomass boilers have been well developed and reached a high quality and performance level in Europe with main focus on optimization of boiler energy efficiency and reducing harmful emissions as much as possible [6]. The usage of wood pellets for the provision of residential space heating and domestic hot water has become more popular in Europe in last decade [7]. A wide range of modern pellet boilers are available in the European market [8]. Pellet boilers are devices which cause the lowest emissions of air pollutants compared to other solid fuel boilers [9]. Although the combustion of biomass can be considered as neutral regarding carbon dioxide (CO_2) emissions [10], further boiler improvements are still needed in order to meet future stricter pollutant emissions limits [11], especially particulate matter (PM), organic gaseous compounds (OGC), carbon monoxide (CO) and nitrogen oxides (NO_X).

Modern small-scale biomass combustion systems are still mostly optimized experimentally with primary measures, e.g., with different techniques via air staging [12,13] or by control of the airflow to the

* Corresponding author.
E-mail address: miguelgr@uvigo.es (M.A. Gómez).

https://doi.org/10.1016/j.enconman.2022.116003
Received 29 April 2022; Received in revised form 20 June 2022; Accepted 11 July 2022
Available online 15 July 2022
0196-8904/© 2022 The Authors. Published by Elsevier Ltd. This is an open access article under the CC BY-NC-ND license (http://creativecommons.org/licenses/by-nc-nd/4.0/).

Nomenclature

A_η	Char oxidation parameter [-]
$A_{i,j}$	Linear equation coefficient [-]
A_j	Area of the j-th grate section [m^2]
B_i	Linear equation independent term [-]
CR	Mass conversion ratio [-]
E_η	Char oxidation parameter [K]
H	Reaction enthalpy [$J{\cdot}kg^{-1}$]
h_i	i-specie combustion enthalpy [$J{\cdot}kg^{-1}$]
h_{fg}	Evaporation enthalpy [$J{\cdot}kg^{-1}$]
h_s	Solid phase enthalpy [$J{\cdot}kg^{-1}$]
k_s	Thermal conductivity of the solid phase [$W{\cdot}m^{-1}{\cdot}K^{-1}$]
K	Kinetic constant [$m{\cdot}s^{-1}$]
K_m	Mass transfer constant [$m{\cdot}s^{-1}$]
LHV	Low heating value [$J{\cdot}kg^{-1}$]
M_k	Molecular weight of the specie k [-]
$\dot{m}$	Mass flow rate [$kg{\cdot}s^{-1}$]
$\dot{Q}$	Heat flux [W]
S	Source term [$W{\cdot}m^{-3}$]
t	Time [s]
T	Temperature [K]
v	Velocity [$m{\cdot}s^{-1}$]
V	Volume [m^3]
Y_j	Mass fraction of the j^{th} biomass component [-]

Greek Symbols

γ_k	Mass fraction of the k^{th} volatile species generated in the bed [-]
ε	Solid fraction [-]
η	Char oxidation stoichiometric parameter [-]
ρ_p	Particle density [$kg{\cdot}m^{-3}$]
$\dot{\omega}''$	Specific rate of generation or consumption [$kg{\cdot}m^{-3}{\cdot}s^{-1}$]

Subscripts

i,j,k	Species indexes or grate section index
PA	Primary air
$sens$	Sensible heat
rad	Radiation
$conv$	Convection
$react$	Reaction
dry	Drying
dev	Devolatilization
ox	Oxidation
g	Gas
v	Volatiles
c	Char

Superscripts

dev	Devolatilization
db	Dry based
ox	Oxidation

boiler using a model-based nonlinear predictive controller [14]. Since it is difficult and costly to fully optimize the boiler experimentally [12], Computational Fluid Dynamics (CFD) simulations are of paramount importance for reaching an optimal design and operation of it. However, CFD is a cost-effective tool for studying biomass combustion process and analyzing combustion systems in more details with its optimization [10,15–17] for achieving higher combustion efficiency and lower emissions. Consequently, numerous authors have developed and proposed different CFD modelling approaches/strategies with using adequate sub-models [18,19]. Zero- and one-dimensional sub-models based predominantly on empirical correlations [20,21], fuel bed experimental measured data [22] or on biomass thermal conversion models [23] which can be easily coupled with the CFD via interface allowing mass and energy exchanges between the fuel bed and the freeboard region but this approach cannot predict the state of the solid fuel bed. In case of realistic characterization with individually tracking each solid fuel particle inside the fuel bed, it is necessary to use Lagrangian models such as the discrete element method (DEM) [24,25] or the discrete phase model (DPM) [26] which is coupled with biomass thermal conversion models but high computational resources are required. Eulerian multidimensional models [27–30] require much lower computational resources than Lagrangian models but are more comprehensive approach than zero- and one-dimensional models which usually consider two zones, i.e., the fuel bed defined as a porous medium where the solid and gas phases coexist and the freeboard region set as a simple fluid, allowing dynamic coupling between both phases. Although these models do not treat the fuel bed as individual particles, physics algorithms can be added to simulate the movements and compaction of the solid fuel inside the combustion systems [10]. In general, only carefully selected appropriate sub-models within the selected CFD modelling approach can offer enough reliable results.

This work presents a detailed description of two different steady bed thermal conversion models as efficient strategies for the CFD simulation of biomass domestic boilers and compares their performance on the simulation of a 60-kW boiler. The first one is a 1D bed model that bases the conversion distribution on experimental measurements and the second one a 3D analytical model that locally calculates the thermal conversion based on the particle temperature and the oxygen availability. In addition, both models are tested with four different correlations that model the char oxidation. The bed models and char correlations are applied to the simulation of two different tests of the boiler at 30 and 60 kW of power to compare their operating. This comparison is performed through the analysis of contours of the flame temperature, volatile gases and carbon monoxide contours in the freeboard and the main experimental measurements of power generated and flue gases emission.

The two models compared in this work are two commonly used strategies in the simulations of domestic and industrial boilers with a reasonably low computational cost. The reason to apply them to a boiler working at full- and half-load conditions is because, in the authoŕs experience, some models can give good results when the combustion conditions are favourable (full load) but not when the conditions are not favourable (half load). It is typical that a well-designed boiler has a high thermal efficiency (about 90 %) and low unburnt species, especially CO, when it operates with a high energy density and enough air supply. This is predicted by most models that manage to burn correctly and complete the combustion of all volatiles and CO in the freeboard due to the favorable conditions. However, some models fail when the boilers operate with a lower energy density and lower freeboard temperatures. In that case, the thermal efficiency is lower and the emissions of unburnt species are noticeably higher. Therefore, the models need a higher accuracy to give good predictions.

2. Models description

In this section, two different models based on two of the most commonly used approaches for the CFD simulation of packed bed biomass combustion are presented in detail. The first presented model is a 1D experimental method that introduces the products of the biomass thermal conversion through several sections of the bed top surface. The calculations are based on mass and energy balances and experimental determination of the reactive fluxes. The second model is an analytical

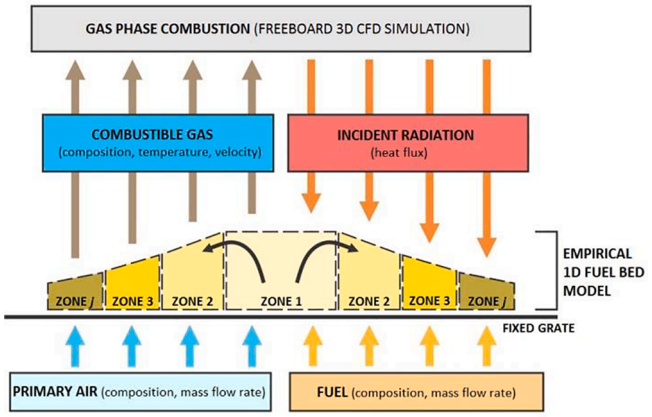

Fig. 1. CFD simulation methodology in empirical bed modelling.

3D method that calculates the packed bed thermal conversion inside the CFD domain. Additionally, the 3D model has an acceptable computational cost for some domestic boilers, especially those with low-size packed beds. However, it can be excessive for boilers with large beds or multi-pass heat exchangers. In such cases, the 1D model can be notably more efficient due to the packed bed simplification and the lower number of species required.

2.1. Empirical 1D bed model

Biomass combustion modelling includes the particle heating-up and conversion sub-processes of drying, devolatilization and char oxidation [31]. A one-dimensional (1D) bed model is commonly used to predict all conversion processes during biomass combustion in a fixed bed. Within the empirical 1D bed model, a several biomass conversion rates (i.e., rate of drying, rate of devolatilization and rate of char oxidation) are prescribed as a function based on experimental measurements or experience [32]. Given such biomass conversion rates, the profiles of temperature, velocity and species mass fraction leaving fuel bed into the freeboard can be calculated based on the overall heat and mass balance of the feedstock, primary air and incident radiation onto each zone [33]. The results of the balances are introduced in the CFD computational domain as boundary conditions of fixed bed top surface. Fig. 1 shows a scheme on the 1D modelling of a circular fixed bed, the parameters used and the fluxes exchanged across the bed boundary condition.

In empirical 1D bed model, the grate is divided in *j*-th individual zones [21]. In each zone, the mass fluxes of moisture, volatiles and char are evaluated by the formulation shown in Equation (1) [34], where the suffix *i* represents fuel moisture, volatiles and char, respectively. $\dot{m}_{i,feed}$ and $CR_{i,j}$ denote the mass flow rate of *i*–th species in the feedstock, and mass conversion ratio of *i*–th species in *j*–th zone of the grate.

$$\dot{m}_{i,j} = \dot{m}_{i,feed} CR_{i,j} \tag{1}$$

The main assumption is that the in-bed combustion of the released volatiles, which is lumped into one single artificial species $CH_xO_yN_z$, is negligible due to the poor mixing and the short residence time of the released volatiles in the fuel bed [34]. During the devolatilization process the chemical reactions (R.1) and (R.2) take place in a two-step combustion scheme.

$$CH_xO_yN_z + aO_2 \rightarrow CO + bH_2O + \frac{z}{2}N_2 \tag{R.1}$$

$$CO + O_2 \rightarrow CO_2 \tag{R.2}$$

The char forms as volatiles escape from the biomass fuel particles. There is a great controversy about the temperature and the products of char oxidation reactions. During the char oxidation by oxygen, a series of intermediate reaction occurs, and the final primary products are CO and CO_2. The CO/CO_2 ratio depends on the local temperature of fuel bed since the activation energies of the reactions differ [35,36]. Further, the CO/CO_2 ratio depends on the concentration of oxygen [37]. The char oxidation reaction is defined as shown in (R.3). This reaction is modelled through a parameter η, that is a function of the CO/CO_2 ratio which varies from 0 for exclusively CO_2 production and 1 for exclusively CO production. Equation (2) shows that parameter which depends on reaction temperature and is evaluated by multiple empirical correlations of the ratio CO/CO_2 available in literature, as Mehrabian et al. summarizes in his study [38]. The assumption, which is sometimes employed in literature, that the combustion of biomass char particles produces only or mainly CO is not suitable, at least for biomass wood pellets and the CO/CO_2 ratio in general strongly depends on the feedstock [39]. Different constants of this correlation are shown in Table 1 and a representation of the CO percentage versus the particles temperature of the different formulations is shown in Fig. 2. In the present paper, these three formulations and another one that considers all the char reacts to CO ($\eta = 1$) are applied for char oxidation equation with the two packed bed models.

Table 1
The most commonly employed CO/CO_2 correlations in literature.

Name of CO/CO_2 empirical correlation	A_η	E_η
Arthur [41]	2511	6240
Evans and Emmons [42]	4.3	3390
Pedersen [43]	12	3300

Parameters such as CO oxidation rate and bed temperature are also important for the results. The study of different CO oxidation kinetics can contribute to a better understanding and to choose the optimum formulation in the application range. However, as that study would be excessively extensive, in this work the CO oxidation rate is modelled through the expression proposed by Westbrook and Dryer [40] for two-step reaction mechanisms shown below (Equation (3)), which has been commonly used for numerical biomass combustion works. On the other hand, the bed temperature is locally calculated through the enthalpy transport equations for the 3d-bed model and through the energy balance for the 1d-bed model.

$$Char + \left(1 - \frac{\eta}{2}\right) O_2 \rightarrow \eta CO + (1-\eta) CO_2 \tag{R.3}$$

$$\eta = \frac{\frac{CO}{CO_2}}{1 + \frac{CO}{CO_2}} = \frac{A_\eta \bullet exp(-E_\eta/T)}{[1 + A_\eta \bullet exp(-E_\eta/T)]} \tag{2}$$

$$k_{CO} = 2.239 \cdot 10^{12} \exp\left(-\frac{1.7 \cdot 10^{8}}{RT}\right) \tag{3}$$

The value of η also depends on the amount of oxygen available. In case if the oxygen is limited, the char is not allowed to react to CO_2. So, η must be higher than certain value shown in Equation (4). Therefore, the value of η must be calculated as shown in Equation (5).

$$\eta \geq \frac{2 \bullet \dot{m}_{char,j} \bullet M_O - \dot{m}_{PA,j} \bullet Y_{O_2,PA} \bullet M_C}{\dot{m}_{char,j} \bullet M_O} \tag{4}$$

$$\eta = max\left\{ \frac{A_\eta \bullet exp(-E_\eta/T)}{[1 + A_\eta \bullet exp(-E_\eta/T)]}, 2\left[1 - \frac{\dot{m}_{PA,j} \bullet Y_{O_2,PA}}{\dot{m}_{char,j} \bullet \frac{2M_O}{M_C}}\right] \right\} \tag{5}$$

Mass flow of Carbon Monoxide (CO) and Carbon Dioxide (CO_2) from individual *j*-th zone into furnace is dependent on η parameter which is calculated as Eqs. (6) and (7) indicate and mass flow of O_2 and N_2 from each individual zone into furnace is defined as shown in Eqs. (8) and (9). In these equations, $\dot{m}_{PA,j}$ is mass flow of primary air (PA) in *j*-th zone of the grate, $Y(O_2)_{PA}$ and $Y(N_2)_{PA}$ represent mass fraction of O_2 and N_2 in PA in %wt, M_O and M_C are molar mass of carbon and oxygen.

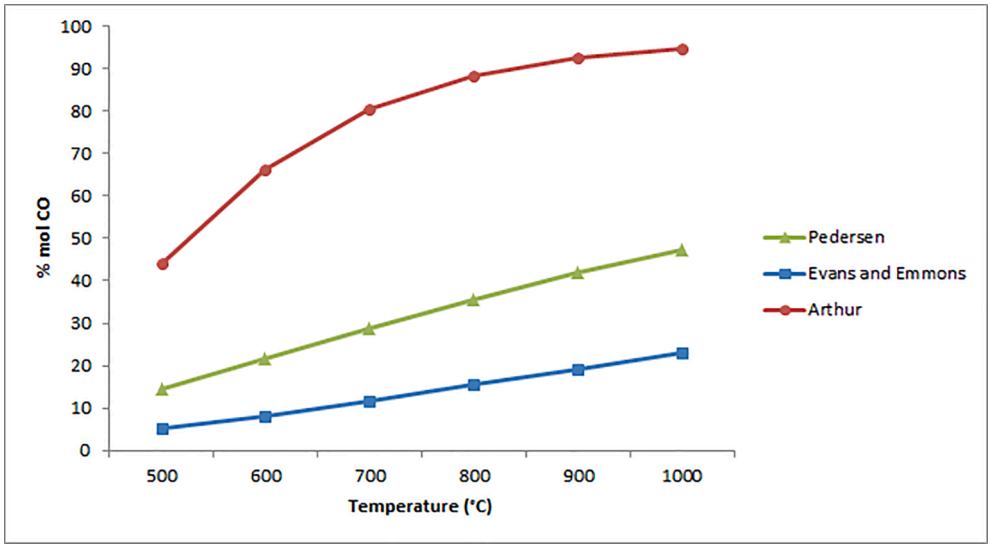

Fig. 2. Predicted CO mol percentage during char oxidation by different CO/CO_2 correlations available in literature.

$$\dot{m}_{CO,j} = \eta \cdot \dot{m}_{char,j} \cdot \frac{M_C + M_O}{M_C} \tag{6}$$

$$\dot{m}_{CO_2,j} = (1-\eta) \cdot \dot{m}_{char,j} \cdot \frac{M_C + 2M_O}{M_C} \tag{7}$$

$$\dot{m}_{O_2,j} = \dot{m}_{PA,j} \cdot Y_{O_2,PA} - \left(1 - \frac{\eta}{2}\right) \cdot \dot{m}_{char,j} \frac{2M_O}{M_C} \tag{8}$$

$$\dot{m}_{N_2,j} = \dot{m}_{PA,j} \cdot Y_{N_2,PA} \tag{9}$$

The total mass flux of the gas mixture into the freeboard in j–th section of the grate can be calculated as shown in Eq. (10), as well as the char oxidation heat from individual zone into freeboard is calculated as Eq. (11), where the heat released during partial oxidation of a kilogram char, $H_{i,char}$, is shown in Eq. (12) where h_{CO} and h_{CO_2} represent enthalpy of formation ($h_{CO} = -110.5 kJ/mol$ and $h_{CO2} = -393.5\,\mathrm{kJ/mol}$). Evaporation heat from individual zone into freeboard is formulated as shown in Eq. (13). $\dot{m}_{H_2O,j}$ is mass flow of evaporated moisture content from fuel in individual zone of the grate and h_{fg,H_2O} is the specific enthalpy change of evaporation ($h_{fg} = h_g - h_f$;, hg is the specific enthalpy of saturate steam, h_f is the specific enthalpy of liquid water).

$$\dot{m}_{g,j} = \dot{m}_{H_2O,j} + \dot{m}_{volatile,j} + \dot{m}_{CO,j} + \dot{m}_{CO_2,j} + \dot{m}_{O_2,j} + \dot{m}_{N_2,j} \tag{10}$$

$$\dot{Q}_{charOx,j} = H_{i,char} \cdot \dot{m}_{char,j} \tag{11}$$

$$H_{i,char} = -\frac{\eta \cdot h_{CO} + (1-\eta) h_{CO_2}}{M_C} \tag{12}$$

$$\dot{Q}_{evap,j} = -\dot{m}_{H_2O,j} \cdot h_{fg,\ H_2O} \tag{13}$$

The amount of sensible heat (feedstock, PA) in each j-th zone of the grate is defined as shown in equation (14), where $Y_{(O_2,N_2),PA}$ is mass fraction of individual component in PA in %wt, $C_{p_{(O_2,N_2),PA}}$ is mean c_p of individual species in PA stream, T_{PA} and T_{feed} are inlet PA temperature and inlet (feeding) temperature of feedstock. Finally, gas temperature $T_{g,j}$ and velocity $v_{g,j}$ into the freeboard in j–th section of the grate can be calculated with Eq. (15) and Eq. (16), respectively, where $c_{p,g}$, $\rho_{p,g}$ and A_j represent specific heat capacity of gas mixture, density of gas mixture and surface area in j-th zone of the grate, among which $\dot{Q}_{rad,j}$ changes with the coupled bed model–freeboard CFD simulation until the coupled simulation is converged.

$$\dot{Q}_{sens,j} = \dot{m}_{PA,j} \cdot \left(Y_{O_2,PA} \cdot C_{pO_2,PA} + Y_{N_2,PA} \cdot C_{pN_2,PA}\right) \cdot \left(T_{PA} - T_{feed}\right) \tag{14}$$

$$T_{g,j} = \frac{\dot{Q}_{charOx,j} + \dot{Q}_{sens,j} + \dot{Q}_{evap,j} + \dot{Q}_{rad,j}}{\dot{m}_{g,j} \cdot c_{p,g}} + T_{feed} \tag{15}$$

$$v_{g,j} = \frac{\dot{m}_{g,j}}{\rho_{g,j} \cdot A_j} \tag{16}$$

2.2. Analytical 3D bed model

This model simulates the boiler in a steady state, which is quicker than transient models, but simulates the thermal conversion of the packed bed with a higher accuracy than most of the steady models. The packed bed is simulated as a porous region and the temperature of the solid particles is defined as a User Define Scalar (UDS) to be distinguish from the gas temperature. The thermal conversion of biomass is based on the solid phase temperature and the mass, energy and species generated during the conversion are introduced in the gas phase as source terms through User Defined Functions (UDF).

2.2.1. Solid phase

The packed bed is modelled as a porous zone in which several sources are introduces to represent the gases and energy released during thermal conversion. The bed is represented in the computational domain as a cell zone. This means it has to be modelled and meshed, so, the shape of the packed bed has to be known previously to apply the model. The porous zone is modelled considering a spherical equivalent particle with an average porosity defined in the fuel description section. In addition, a momentum source is introduced in the gas phase through the Ergun's equation [44] and the definition of the viscous and inertial resistance as shown in [30].

In most models, the thermal conversion is commonly controlled by the particles temperature. Therefore, it is necessary to difference the temperature of solid phase and gas phases. To achieve this, a variable that represents the solid phase enthalpy is introduced as a UDS in the packed bed region and a transport equation (Equation (17)) has to be solved to calculate the temperature. The parameters and coefficients of this equation have to be introduced in the different terms to solve the value of enthalpy and the corresponding temperature. As this model works in steady state, the left hand of the equation is null and only the thermal conductivity and the source term have to be introduced in the CFD code. The thermal conductivity of the bulk packed bed was

Table 2
Kinetics of biomass thermal conversion reactions.

Solid phase reactions		Kinetics
Dry wood→Gas	(R.4)	$K_{gas} = 111{\cdot}10^{9}\exp\left(-\frac{177{\cdot}10^{3}}{RT_s}\right)$
Dry wood→Tar	(R.5)	$K_{tar} = 9.28{\cdot}10^{9}exp\left(-\frac{149{\cdot}10^{3}}{RT_s}\right)$
Dry wood→Char	(R.6)	$K_{char} = 30.5{\cdot}10^{9}exp\left(-\frac{125{\cdot}10^{3}}{RT_s}\right)$
Char→ CO, CO_2 (same as (R.3))		$K_{ox} = 1.715 \cdot T_s{\cdot}exp\left(-\frac{9000}{T_s}\right)$

measured at 0.17 W/m·K. The source term, shown in Equation (18) is an addition of three terms that include heat exchanged through radiation and convection and the heat generated by the fuel reactions. The radiation and convection terms are introduced as shown in the authors previous work [45]. The radiative heat transfer is modelled through a modification of the Discrete Ordinates (DO) Model to make the packed bed participative in radiation as a semi-transparent medium. This is achieved through several source terms of the solid and gas energy equations and the modification of the absorption coefficients as detailed in [46]. The convection heat exchange with the gas phase is modelled through the Wakao correlation for the heat transfer coefficient [47]. The reactive term (Equation (19)) considers the energy released during devolatilization and char oxidation in the cell. The devolatilization energy is considered as the difference of the Lower Heating Value (LHV) in dry basis of the fuel and the enthalpies of reaction of the released volatile gases and the generated char, as shown in Equation (20). The char reactive term (Equation (21)) considers the fractions of char oxidized to CO and to CO_2. Both, devolatilization and char reactive source terms are scaled by the mass flow rates of devolatilazed biomass and consumed char in the cell, whose formulations are shown below.

$$\frac{\partial(\varepsilon\rho_p h_s)}{\partial t} = \nabla(k_s{\cdot}\nabla T_s) + S_{h_s} \tag{17}$$

$$S_{h_s} = S_{rad} + S_{conv} + S_{react} \tag{18}$$

$$S_{react} = S_{react}^{dev} + S_{react}^{char} \tag{19}$$

$$S_{react}^{dev} = \dot{\omega}_{dev}^{'''}\left(LHV_{fuel}^{db} + h_{dev} - \frac{Y_v}{Y_v + Y_c}\sum_j \gamma_j h_j - \frac{Y_c}{Y_v + Y_c}h_{char}\right) \tag{20}$$

$$S_{react}^{char} = \dot{\omega}_{char}^{'''}[\eta{\cdot}h_{char\ to\ CO} + (1-\eta)h_{char}] \tag{21}$$

The fuel thermal conversion rates are modelled in a simple way since the model calculates the boiler operation in steady state. Drying, devolatilization and char reaction rates are calculated by scaling the incoming fuel mass flow rate by the fractions of moisture, volatile and char fractions obtained in the proximate analysis of the fuel. Equations (22), (23) and (24) show, respectively, the rates drying, devolatilized and char consumed mass in the computing cells. Whereas the drying process is assumed to be homogeneous in the bed, the rates of devolatilizated fuel and consumed char are scaled through pyrolysis kinetic coefficients and the char global oxidation coefficient. This way, the devolatilization and char reactive fronts are mainly located in those cells in which the temperature favour the kinetics.

$$\dot{\omega}_{dry}^{'''} = \frac{\dot{m}_{fuel}}{V_{bed}}{\cdot}Y_m \tag{22}$$

$$\dot{\omega}_{dev}^{'''} = \frac{\dot{m}_{fuel}}{V_{bed}}{\cdot}(Y_v + Y_c)\frac{K_{dev}{\cdot}V_{cell}}{\sum_1^{n_{cells}}(K_{dev}{\cdot}V_{cell})} \tag{23}$$

$$\dot{\omega}_{char}^{'''} = \frac{\dot{m}_{fuel}}{V_{bed}}{\cdot}Y_c\frac{K_{ox}^{global}{\cdot}V_{cell}}{\sum_1^{n_{cells}}(K_{ox}^{global}{\cdot}V_{cell})} \tag{24}$$

The kinetics of the pyrolysis reactions to volatile light gases, tars and char, and char oxidation are shown in Table 2 (R.4), (R.5), (R.6) and char reaction (R.3), respectively. These reactions are modelled using the flash kinetics proposed by Wagenaar et al [48] and the char oxidation kinetics proposed by Bryden and Ragland [49]. On the one hand, the overall devolatilization kinetic coefficient is formulated as the addition of the three pyrolysis reaction kinetics (Equation (25)). On the other hand, the global char oxidation coefficient, shown in Equation (26), makes the reaction controlled both through oxygen diffusion and the reaction (R.3) kinetics, this means both processes will limit reaction rate of char consumption. The mass transfer rate (K_m^{ox}) in Equation (26) is calculated in an analogous formulation to the convection coefficient [45].

$$K_{dev} = K_{gas} + K_{tar} + K_{char} \tag{25}$$

$$K_{ox}^{global} = \frac{1}{\frac{1}{K^{ox}} + \frac{1}{K_m^{ox}}} \tag{26}$$

Gas phase.

CFD codes are highly developed to solve the single phase fluid dynamics including gas phase homogeneous combustion. The physical processes of flow, reaction and heat transfer occurring in a boiler freeboard can be efficiently simulated by using the models that CFD codes offer. Therefore, the main difficulty on the gas phase modelling when a biomass boiler is simulated is the interaction with the packed bed and the gas species reaction scheme. The multiple volatile species that are released from a reacting biomass bed are assumed to be represented by a few representative species that can be simulated without an excessive computational effort. Those volatile species can be grouped in heavy hydrocarbons represented by benzene (C_6H_6), light hydrocarbons represented by methane (CH_4) and other common gaseous species such as, H_2, H_2O, CO, and CO_2.

The gas species are released from the bed during the thermal conversion. These species are introduced in the computational domain as volumetric sources in the packed bed porous region. So, the key is to calculate the mass flow rates of each specie. All the gas species sources are based on the thermal conversion rates shown in equations (22), (23) and (24). As H_2O is released from drying and devolatilization, its mass flow rate (Equation (27)) includes the drying term and the devolatilization rate scaled by the corresponding mass fraction γ_{H_2O}. C_6H_6, CH_4, H_2 are produced during pyrolysis, so, their released rates are the devolatilization rate scaled by the corresponding fraction γ_k (Equation (28)). The calculation method to obtain the mass fractions of the volatile species produced during pyrolysis is shown below. Last, the mas flow rates of the released CO and CO_2 (Equations (29) and (30), respectively) are calculated by considering both, the char oxidation reaction (R.3) stoichiometry and the corresponding devoltilization rates.

$$\dot{\omega}_{H_2O}^{'''} = \dot{\omega}_{dry}^{'''} + \dot{\omega}_{dev}^{'''}\,\gamma_{H_2O} \tag{27}$$

$$\dot{\omega}_{vol\ k}^{'''} = \dot{\omega}_{dev}^{'''}\,\gamma_k \tag{28}$$

$$\dot{\omega}_{CO}^{'''} = \dot{\omega}_{char}^{'''}{\cdot}\eta\frac{M_{CO}}{M_C} + \dot{\omega}_{dev}^{'''}\,\gamma_{CO} \tag{29}$$

$$\dot{\omega}_{CO_2}^{'''} = \dot{\omega}_{char}^{'''}{\cdot}(1-\eta)\frac{M_{CO_2}}{M_C} + \dot{\omega}_{dev}^{'''}\,\gamma_{CO_2} \tag{30}$$

The homogeneous gas reactions can be modelled through a simple reaction scheme that represent the overall combustion. This scheme has already been by the authors in previous papers [27,45,50]. It is based on the oxidation of the hydrocarbons into carbon monoxide and water (R.7), (R.8) and (R.9), the oxidation of carbon monoxide (R.10) and a two-way reaction of carbon monoxide with water, (R.11).

$$C_6H_6 + \frac{9}{2}O_2 \rightarrow 6\ CO + 3\ H_2O \tag{R.7}$$

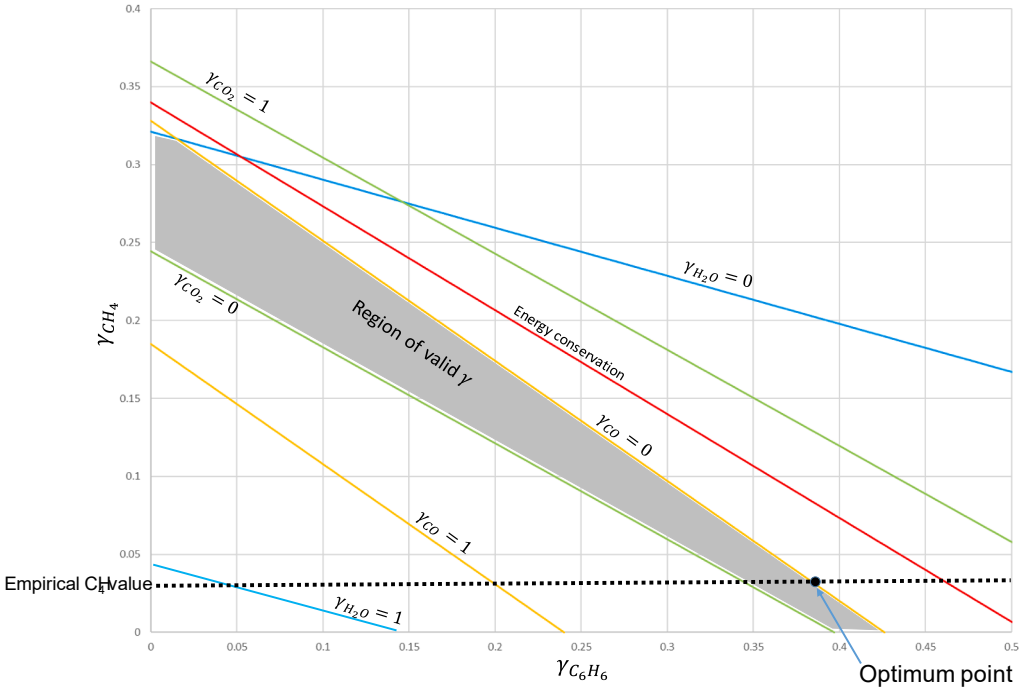

Fig. 3. Diagram of γ representation for the fuel 2 devolatilizing at a temperature of 750 K with the region of valid γ and the optimum point shown.

$$CH_4 + \frac{3}{2}\ O_2 \rightarrow CO + 2\ H_2O \quad \text{(R.8)}$$

$$H_2 + \frac{1}{2}O_2 \rightarrow H_2O \quad \text{(R.9)}$$

$$CO + \frac{1}{2}O_2 \rightarrow CO_2 \quad \text{(R.10)}$$

$$H_2O + CO \rightleftarrows CO_2 + H_2 \quad \text{(R.11)}$$

Composition of volatile gases.

One of the main challenges in the field biomass pyrolysis modelling is the representation of the volatile compounds, from models that consider one unique volatile specie to multiple compounds. As the present model uses a few gas species that represent the great variety of compounds present in a real process, it is complex to find a combination of those volatile species that is consistent with the fuel composition, the kinetics of devolatilization and the chemical energy conservation. A well-known method to find the composition of volatiles is the one published by Thunman and Leckner [51] and similarly by Neves et al. [52] in which they apply linear equation systems based on species and energy conservation as well as empirical correlations to find the set of mass fractions of the volatile species. This returns a fixed volatile composition for each fuel, however, its mass fractions values are commonly negative or higher than one. Based in a similar approach, in the present work we propose a solution that returns a realistic solution for most fuels and pyrolysis kinetics. The method searches a solution that fulfils mass conservation and minimizes the chemical energy conservation, whose energy error can be compensated with the devolatilization energy source (Equation (20)). The mass conservation for carbon, hydrogen and oxygen is stated in the linear equation system (31). In this case, hydrogen mass fraction was set to 0 to simplify the resulting system to 2 unknowns, which can be easily represented in a 2D diagram, since hydrogen is a minority species in the volatile gases set. As the rank of the matrix associated with the system is 3 and we consider 5 volatile species, all species mass fractions can be represented as a linear combination of two of them. In Eq. (32) γ_{H_2O},γ_{CO} and γ_{CO_2} are shown as linear functions of γ_{CH_4} and $\gamma_{C_6H_6}$ being A_{ij} and B_i constant values. Therefore, all possible

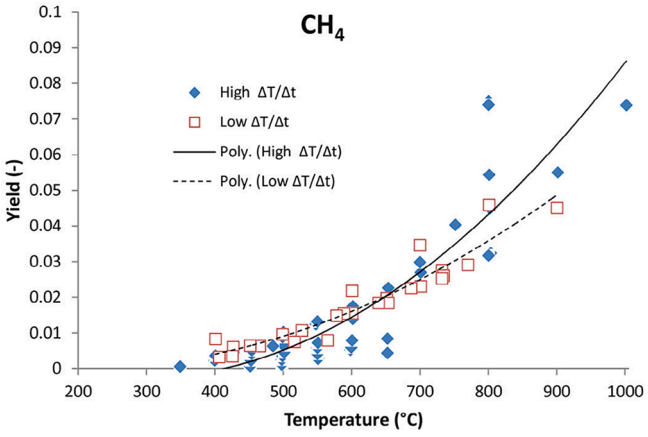

Fig. 4. Experimental adjust for γ_{CH_4} as a function of temperature [53].

combinations of γ_k can be represented in a plane as a function of γ_{CH_4} and $\gamma_{C_6H_6}$. In that plane the functions $\gamma_k = 0$ and $\gamma_k = 1$ (for k = CO_2, CO and H_2O) are straight lines, as represented in Fig. 3. For most biomass fuel compositions, it is possible to find a region that fulfils that all mass fractions γ_k are between 0 and 1. That is the region of valid γ represented in Fig. 3. To find a point in the region of valid γ, an experimental correlation can be used to set a value of γ_{CH_4} as a function of temperature. In the present work, that correlation of γ_{CH_4} was extracted from the literature review presented by Anca-Couce [53] based on the data shown in Fig. 4. In that work, CH_4 seems to be the specie that shows a lower dispersion to set an adjusted function. The last condition to find the optimum point is the energy conservation condition: As Equation (33) shows, the reaction enthalpy of the volatiles and char produced has to equal the LHV (dry basis) of the fuel plus the devolatilization enthalpy. Again, all γ_j can be written as a linear combination of of γ_{CH_4} and $\gamma_{C_6H_6}$. Therefore, the energy conservation equation can also be represented as a linear function (Equation (34)) in Fig. 4. Then, if the energy conservation line crossed the γ_{CH_4} constant line inside the region of valid γ, that

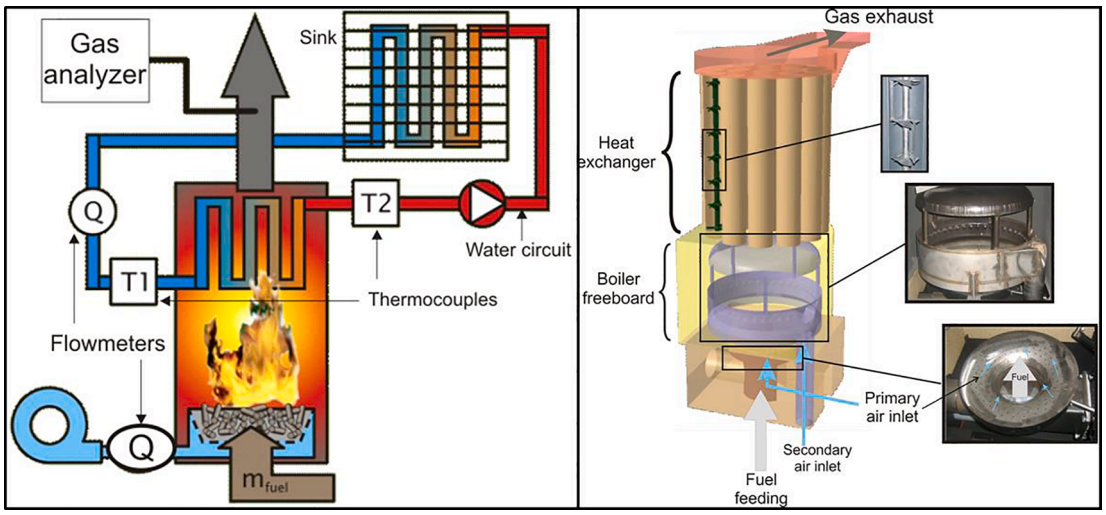

Fig. 5. Schematic of the experimental plant [27].

crossing point would fulfil mass, species and energy conservation. As this is not usual for most fuel compositions, the closer point (in this case matches the line of $\gamma_{CO} = 0$ can be considered the optimum point since it fulfils carbon, hydrogen and oxygen mass conservation, the γ_{CH_4} empirical value and the minimum error of energy. This error in energy conservation is corrected by the energy source shown in Equation (20). All lines shown in Fig. 3 depend on the fuel composition of carbon, hydrogen and oxygen and temperature. Therefore, for some fuel compositions or kinetics it is not possible to find region of valid γ with these volatile species. Nevertheless, for most types of wood biomass and wood kinetics the region commonly is found when devolatilization temperature is higher than 600 K.

$$\begin{pmatrix} 0 & \frac{1}{M_{CO}} & \frac{1}{M_{CO_2}} & \frac{1}{M_{CH_4}} & \frac{6}{M_{C_6H_6}} \\ \frac{2}{M_{H_2O}} & 0 & 0 & \frac{4}{M_{CH_4}} & \frac{6}{M_{C_6H_6}} \\ \frac{1}{M_{H_2O}} & \frac{1}{M_{CO}} & \frac{2}{M_{CO_2}} & 0 & 0 \end{pmatrix} * \begin{pmatrix} \gamma_{H_2O} \\ \gamma_{CO} \\ \gamma_{CO_2} \\ \gamma_{CH_4} \\ \gamma_{C_6H_6} \end{pmatrix} = \begin{pmatrix} Y_{C,vol} \\ Y_{H,vol} \\ Y_{O,vol} \end{pmatrix} \tag{31}$$

$$\begin{pmatrix} \gamma_{H_2O} \\ \gamma_{CO} \\ \gamma_{CO_2} \end{pmatrix} = \begin{pmatrix} A_{11} & A_{12} \\ A_{21} & A_{22} \\ A_{31} & A_{32} \end{pmatrix} * \begin{pmatrix} \gamma_{CH_4} \\ \gamma_{C_6H_6} \end{pmatrix} + \begin{pmatrix} B_1 \\ B_2 \\ B_3 \end{pmatrix} \tag{32}$$

$$Y_v \sum_j \gamma_j h_j = LHV^{db}_{fuel} + h_{dev} - Y_c h_{char} \tag{33}$$

$$A_{41} \cdot \gamma_{CH_4} + A_{42} \cdot \gamma_{C_6H_6} = B_4 \tag{34}$$

3. Experimental system

3.1. Boiler

The presented models were applied in two tests performed in a commercial boiler with different fuels and operating conditions. The boiler was previously used in other studies presented by the authors [27,30]. The plant is equipped to measure the power transferred to the water, the temperature of fumes and the contaminant emissions, shown in Fig. 5. The boiler is appropriate to difference the packed bed thermal conversion, the gas homogeneous reactions and the fumes heat exchange since the three regions are clearly separated. The bed is located in the lower part of the boiler and fuel rises through a volcano-type system to a circular grate in which the primary air is injected. Over the bed the secondary air in injected through a blowing ring that feeds the volatile gases released from the bed to create a flame confined zone that is covered by a dome. This prevents the flame from reaching the heat exchanger which can produce a flame quenching that produces a high content of unburnt species. The heat exchanger is formed by fifteen tubes that cross the water chamber. These tubes contain flanges that induce a swirl motion to the hot gases that increase the heat exchange. The boiler furnace is also surrounded by the water chamber, which absorbs a great part of the heat released in the volatiles reaction zone mainly though radiation.

Table 3
Fuel properties and analysis results.

Fuel type	Fuel 1	Fuel 2
Proximate Analysis [wet basis % (wt %), as received (a.r.)]		
Moisture	6.8	8.5
Ash	0.44	0.62
Fixed Carbon (char)	24.4	16.2
Volatile matter	68.5	74.7
Properties		
LHV [MJ/kg, a.r.]	16.17	16.56
Equivalent formulation	$CH_{1.57}O_{0.74}N_{0.0025}$	$CH_{1.55}O_{0.59}N_{0.0028}$
Density (approx.) [kg·m^{-3}]	1200	1200
Solid fraction	0.56	0.57
Cylindrical diameter [mm]	6.5	6
Average length [mm]	10.8	11.5
Elementary analysis [dry basis %, ash free]		
C (%)	47.21	52.08
H (%)	6.19	6.75
O (%)	46.46	41.00
N (%)	0.14	0.17

3.2. Fuel

Two different tests are simulated in this work; each test was performed with a different fuel. These fuels are pinewood pellets with different compositions and slightly different morphological properties (listed in Table 3). Although both fuels have similar in physical properties and heating power, the main differences are the volatile and char content and elementary composition. These data are important to calculate the thermal conversion release rates and the volatile gases composition, respectively, in the numerical models.

3.3. Tests

In this work, two different experimental tests are simulated with the mentioned thermal conversion and char reaction models. These two

Table 4
Experimental tests operating conditions.

Experimental test	T1	T2
Operating conditions		
Fuel	Fuel 1	Fuel 2
Fuel feeding rate (g·s-1)	2.26	4.10
Fuel equivalent power (kW)	36.6	67.9
Primary air flow rate (g·s-1)	4.7	10.4
Secondary air flow rate (g·s-1)	9.6	14.5
Air infiltration flow rate (g·s-1)	20.6	10.2
Water temperature (C)	70	70
Measurements		
Power transferred to water (kW)	29.90	60.14
Fumes temperature (C)	196	195
CO_2 in fumes (%) [measured at 10% O_2]	9.74	10.73
CO in fumes (ppm) [at 10% O_2]	227.2	5.6

tests were performed under different operating conditions of thermal power, fuel and air distribution. Table 4 shows the details of the boiler operating conditions. In the test 1 the boiler works at half load, which means 30 kW effective, approximately, and the test 2 at full load (60 kW). The primary, secondary air and infiltrations measured change drastically with the tests, as shown in Table 4. As the air infiltrations are unavoidable and difficult to locate, all the infiltration fluxes are simplified to a mass flow rate located at the bottom of the boiler since it is the region were most gates and moving parts of the boiler shell are placed. The water temperature is 70 ºC for both experiments. All this results are average measurements where the boiler has reached a quasi-steady state.

4. Results and discussion

In this section, the results of all the simulations performed with the described models are shown and compared. The results are divided into two main sections. First, the numerical results on the main parameters of the boiler performance and emissions are compared, and then, the contours of the main variables inside the boiler are analysed. Both analysis give a comparison of the models behaviour on the overall combustion performance, including the deviations respect the experimental measurements, and the freeboard combustion efficiency. Both tests (T1 and T2) previously commented, in which the boiler operates to generate 30 kW and 60 kW (half and full load) of thermal power, respectively, are simulated to take into account the fuel load degree.

4.1. Boiler performance

In order to assess the overall models behaviour to simulate the boiler performance, the parameters measured in the experimental facility are calculated by the predictive models when the steady simulations are converged. These parameters are the heat transferred to water and the measures at the fumes outlet (temperature and CO and CO_2 emissions). Therefore, the two bed models (Empirical 1D and Analytical 3D) and the four char oxidation correlations (Pedersen, Evans & Emmons, Arthur and only CO production) are evaluated through the comparison with the experimental measurements.

4.1.1. Half-load (30 kW) test

As the boiler is designed to operate with a nominal output of 60 kW, the experimental half-load test was performed to transfer to water approximately 30 kW. This test required a fuel mass flow rate of 2.26 g/s (equivalent to approximately 36.6 kW), which means that the boiler operates with an efficiency of 82 %.

The results of the simulations of this half-load test are summarized in the Table 5, as well as the results of the experimental test, which are averaged measured values when the quasi-steady working is reached by the boiler. The Empirical 1D model shows close predictions on the power and fumes temperatures for all char correlations. However, it shows significant differences in the CO and CO_2 emissions. Whereas the Pedersen's and Evans's models show a good agreement with all measured parameters, the Arthur's correlation overpredicts the CO emissions and unburnt volatiles in comparison to Pedersen and Evans correlations. The pure-CO-production model shows excessive CO and low CO_2 emissions, as could be expected and some deviations on power and fumes temperatures. On its part, the analytical 3D model does not show significant differences for the different char correlations. Even the pure-CO-

Table 5
Results of all the simulations with the boiler operating at 30 kW.

30-kW Simulation						
Bed thermal conversion	**Char correlation**	**CO_2 (%)**	**CO (ppm)**	**volatile (ppm)**	**Power to water (kW)**	**Fumes temperature (ºC)**
Empirical 1D model	**Pedersen**	9.79	253.4	12.4	30.2	193.2
	Evans	9.80	214.4	9.0	30.3	193.1
	Arthur	9.87	608.7	65.1	29.7	204.4
	Only CO	9.53	1713.0	272.7	29.1	211.8
Analytical 3D model	**Pedersen**	10.28	188.1	0.6	30.4	168.2
	Evans	10.28	197.6	0.6	30.4	168
	Arthur	10.28	196.9	0.6	30.4	168
	Only CO	10.37	176.7	0.6	30.5	168.4
Experimental		**9.74**	**227.2**	**–**	**29.9**	**196**

Table 6
Results of all the simulations with the boiler operating at 60 kW.

60-kW Simulation						
Bed thermal conversion	**Char correlation**	**CO_2 (%)**	**CO (ppm)**	**volatile (ppm)**	**Power to water (kW)**	**Fumes temperature (ºC)**
Empirical 1D model	**Pedersen**	9.0	0.0	0.0	59.6	218.5
	Evans	9.0	0.0	0.0	59.8	218.5
	Arthur	9.0	0.0	0.0	59.2	219.5
	Only CO	9.0	0.0	0.0	57.9	219.2
Analytical 3D model	**Pedersen**	9.1	0.0	0.0	60.2	193.7
	Evans	9.1	0.1	0.0	60.2	193.7
	Arthur	9.0	0.0	0.0	60.3	193.8
	Only CO	9.0	0.0	0.0	60.3	193.8
Experimental		**10.7**	**6.0**	**–**	**60.1**	**195.0**

production model behaves similar to the other correlations, curiously with lower CO emissions but not significantly different. This model trends to an underprediction on the fumes temperature that may be due to the packed bed radiation to the cooled freeboard walls that transfer a higher power to the water and reduces the fumes sensible enthalpy respect the empirical 1D model. It should be noted that the fouling deposited on the walls of the heat exchanger has not been modelled with high accuracy. This can unbalance the energy transferred to the water and that expelled with the fumes. In any case, for both models, the Pedersen's and Evans & Emmons's correlations show a better behaviour.

4.1.2. Full-load (60 kW) test

The test at full load was performed to transfer to water approximately 60 kW needed a fuel mass flow rate of 4.1 g/s (equivalent to approximately 67.9 kW), giving a boiler thermal efficiency of 88 %.

The results from these simulations of the boiler at full-load operating are summarized in Table 6. In this case, it is remarkable the homogeneity of the char oxidation correlations results for both bed models. Even the pure-CO-production model gives the same data as the other models with the exception of the Empirical 1D model that shows some power loss for that correlation. In the case of the Analytical 3D model all the char correlations give virtually the same results. This is caused due to the high power released in the freeboard that is enough to make react all the volatile species and all released CO in the char oxidation regardless the correlation used. The behaviour of the bed thermal conversion models is also very similar in CO and CO_2 emissions. The Empirical 1D model tends to overpredict the fumes temperature, nevertheless, both models predictions of the thermal power produced are in a good agreement with experimental values.

4.1.3. Char correlations performance

On the one hand, the main conclusion drawn on the char oxidation correlations is that they have not a significant effect when combustion conditions are favourable. The favourable conditions are high temperature and sufficient air supply. This is clear in the full-load test, in which there is a high energy concentration and thus high temperatures in freeboard. This favours the complete reaction of all the volatiles and the CO released from the bed. As a result, the emissions of CO and volatile species are virtually zero, regardless of the bed model or the correlation used. On the other hand, in the half-load test, there is a lower energy concentration in the boiler, which means lower temperatures that difficult the gas combustion. In this case the char correlations play an important role since an excess of CO released from the bed may not be easily consumed in the freeboard and increase the fumes CO emissions. The 1D model is especially sensitive to the char correlations. The better results are obtained with the Evans & Emmons's correlation. The Pedersen's one also give good results. These two correlations produce a low CO proportion which seems to be favourable for the 1D model, probably because they are obtained from experiments with biomass charcoal and their results are more realistic for biomass conversion. For the 3D model the char correlation does not have a significant effect. Curiously, the correlation of pure CO production emits a slight lower CO concentration in the fumes. This may be due to a more aggressive heat release in the flame produced by the addition of the char CO to the volatiles that favours its consumption, which does not happen with the 1D model.

The bed and especially gas temperatures are crucial to control the volatiles reaction rates. That temperature is simulated through the transport equations of the solid and gas phases within the models' capabilities. To verify that the temperatures are correctly simulated, it would require a complex system of measurements in the boiler bed and freeboard, which is not available in the facility. In addition, these temperatures would have to be averaged to be compared with the simulations since they are in steady state. This lack of measurements in the flame zone is considered the main limitation of the present work.

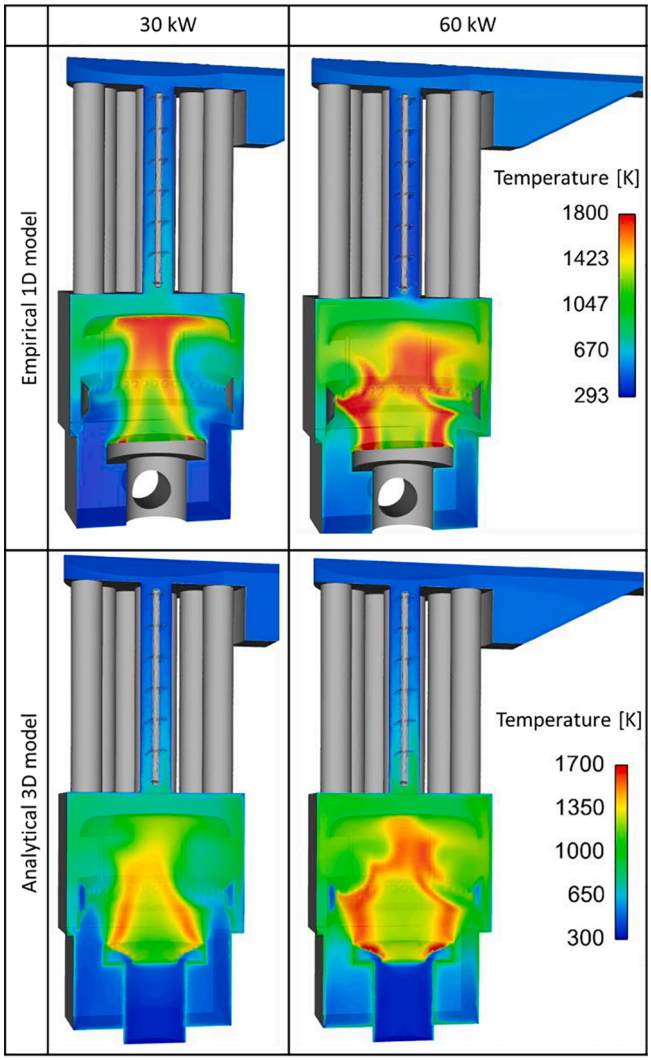

Fig. 6. Comparison of the gas temperature contours in the middle plane from the simulations results of the different bed models.

4.2. Models behaviour

In this section, the both used bed conversion models and char oxidation correlations are compared through the main variables that affect the combustion. The contours of temperatures, carbon monoxide, and volatile species concentrations are shown to analyse the behaviour of the different models.

4.2.1. Effect of the bed thermal conversion model

Fig. 6 shows the temperature contour in the middle plane of the boiler for the simulations of 30 kW and 60 kW with the different bed models. In char oxidation model is used the correlation of Evans & Emmons. The most noticeable difference is the higher global temperature reached by the empirical 1D model. This is caused by the presence of the bed porous zone in the analytical 3D model, which is heated and it emits a high radiation flux due to the absorption/emission coefficient of the solid phase. The 3D simulation of the bed volume also allows the reaction and heats the gases as they are released and the combustion starts in the bed and continues in the freeboard, so it is more progressive. Otherwise, in the 1D model, the gases are released on the top of the bed and have a delay in their heating, then the combustion is more concentrated in the freeboard. As numerical results in the previous section showed, the differences between the models are more significant in 30-kW simulation. Whereas the 3D bed model produces a freeboard

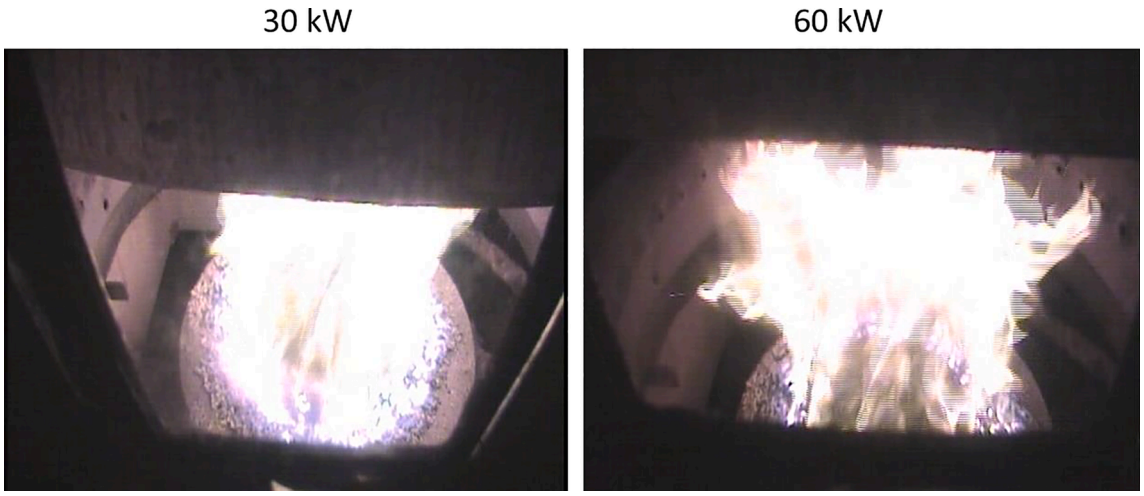

Fig. 7. Captures of the boiler freeboard during the tests.

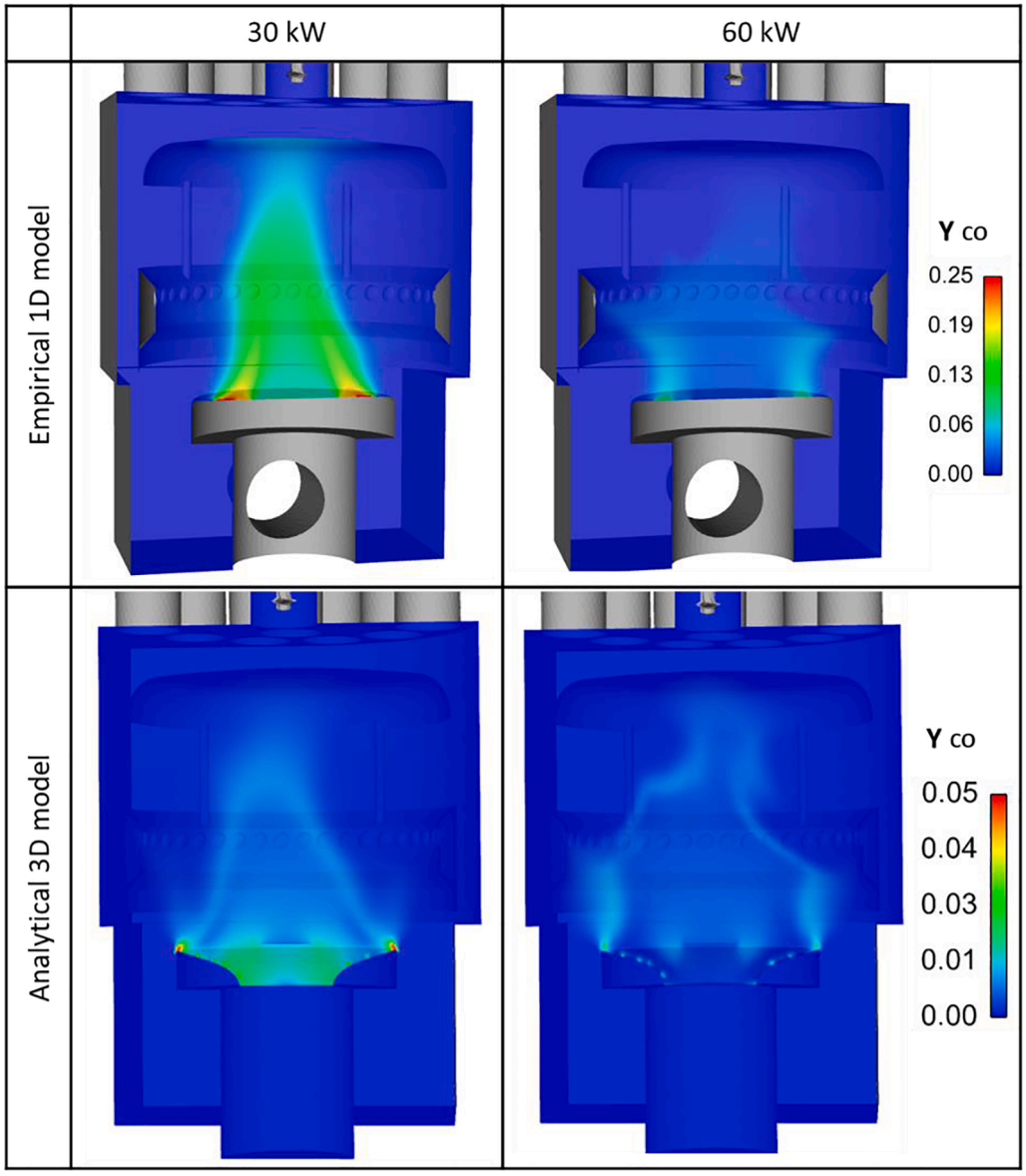

Fig. 8. Comparison of the CO mass fraction contours in the freeboard from the simulations results of the different bed models.

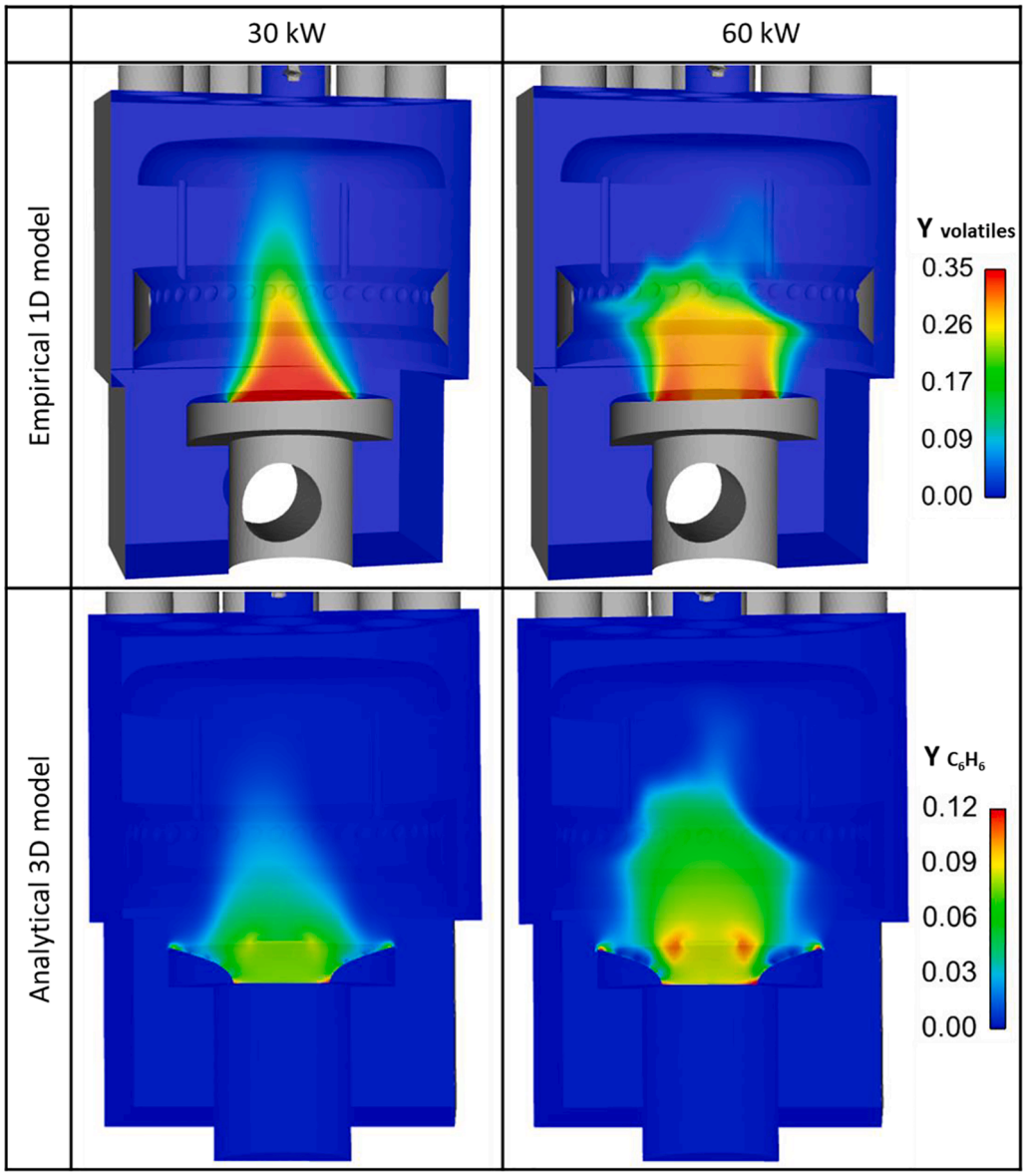

Fig. 9. Comparison of the lumped volatile compound and C_6H_6 mass fractions contours in the freeboard from the simulations results of the different bed models.

temperature more homogeneous, the 1D bed model shows higher temperature gradients inside the freeboard. This is also influenced by the use of several volatile species in the 3D model, which reacts with different kinetics and the reactions are more distributed in the freeboard, while the 1D model represents the volatile gases through one unique lumped specie. Both models predict a similar flame shape which is slimmer for the 30-kW simulation and more voluminous for the 60-kW one.

Fig. 7 shows captures of the flame during the different tests. Despite the fact that the visible flame does not give significant information of the gas temperature, it is interesting to observe the shape which is strongly affected by the secondary air injection in the 60-kW test. In the 30-kW test the flame seems slimmer and more regular.

Other variables that show the combustion performance of a boiler are the concentration of the main combusting species such as CO and volatile hydrocarbons. These are shown in the Figs. 8 and 9, respectively, for the different bed models studied. In Fig. 9, the volatile gases are represented by the lumped volatile specie of the 1D model and C_6H_6 that is the predominant hydrocarbon in the 3D bed devolatilization model. The CO profiles clearly show higher concentrations in the 1D model, especially in the 30-kW test. This reveals a delay in the reaction of CO that needs a higher temperature and the oxygen supply of the secondary air injection to complete the combustion. On the other hand, despite its lower temperature, the 3D model consumes most of the CO in the bed volume, as it is released, and the concentrations found in the freeboard are clearly lower. For the 60-kW test both models predict lower CO concentrations than the 30-kW test. This is caused by the higher energy release that produces a concentration of the reactive gases in the freeboard volume and the higher temperature activates the CO consumption. Fig. 8 shows similar distribution of the volatile concentration for both bed models. The concentrations are not comparable since, whereas the lumped specie groups all the volatile species, the C_6H_6 is only one of the several species released in the 3D bed model. In any case, both tests have a similar behaviour of the volatile species in the freeboard. The 60-kW test produces a more voluminous reacting zone where both, volatiles and CO, are concentrated, due to the higher fuel mass flow rate. This is consistent with the larger flame previously seen in Fig. 6.

4.2.2. *Effect of the char oxidation model*

As the different char oxidation correlations studied in this work produce different CO/CO_2 ratios and energy releases, the contours of CO

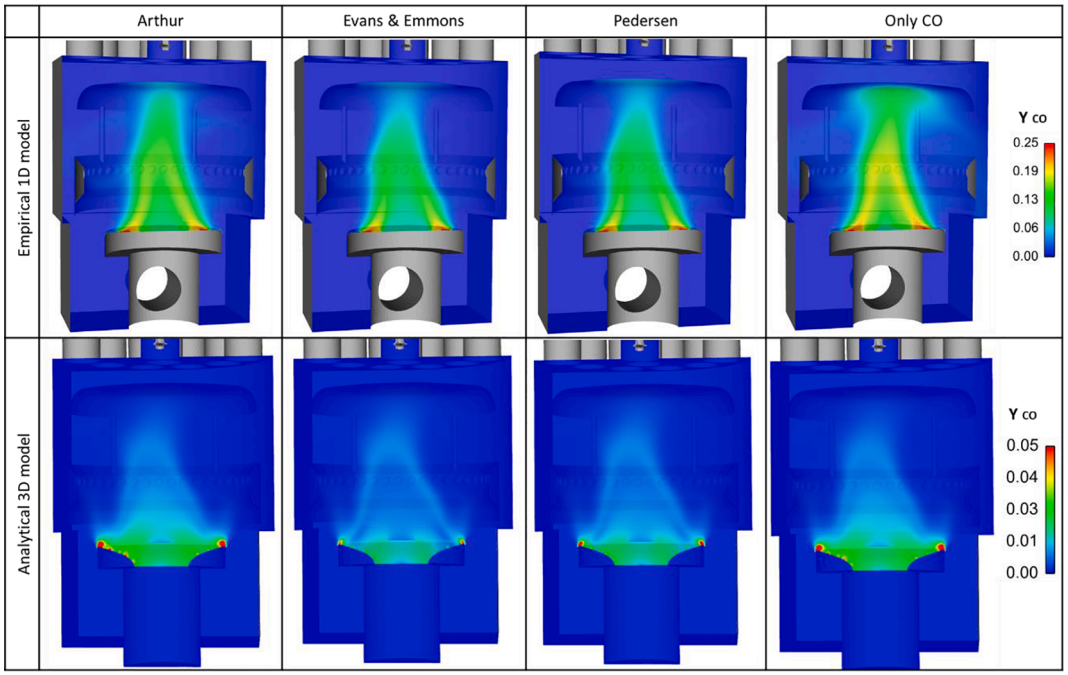

Fig. 10. Contours of CO mass fraction for the different char oxidation correlations and bed models from the 30-kW test simulation.

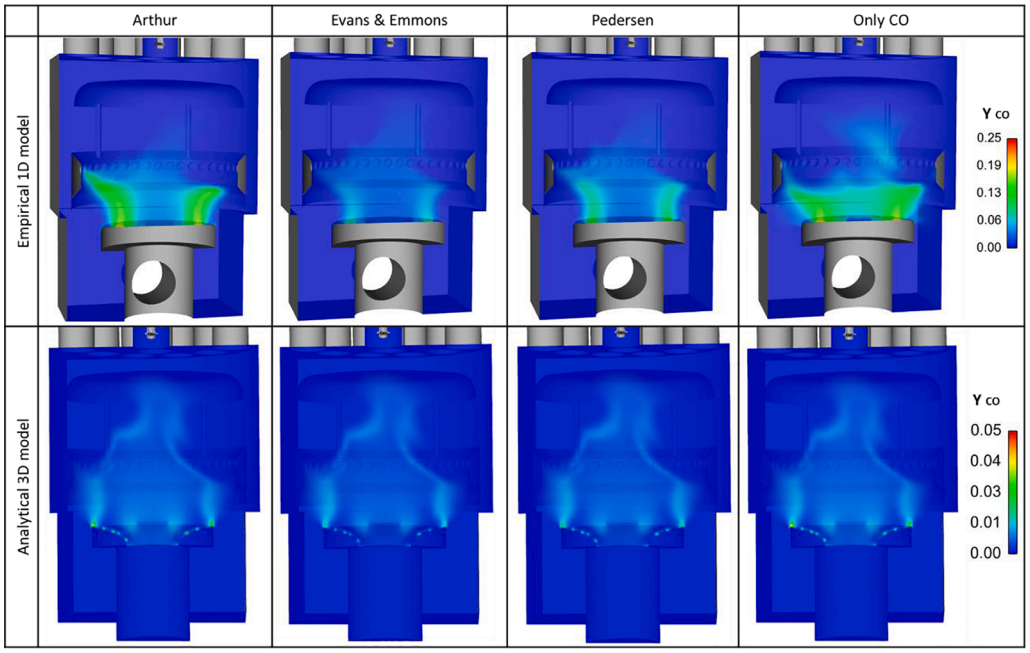

Fig. 11. Contours of CO mass fraction for the different char oxidation correlations and bed models from the 60-kW test simulation.

concentration and temperature are the most significant to analyse the correlations. Figs. 10 and 11 show the CO profiles in the freeboard of the boiler obtained from the different bed models and char oxidation correlations for the 30-kW and 60-kW tests, respectively. The higher production of CO has a noticeable effect when using the 1D bed model since the pure CO production and the Arthur's correlation generate a more elongated CO region in the freeboard than the Evans's and Pedersen's correlations that produces very similar profiles. Otherwise, the analytical 3D model consumes most of the CO in the bed region and the CO profiles in the freeboard are very similar in all cases. The low concentrations find in the 3D model results relates high reactivity that the presence of the bed porous region produces. This is the cause that the char correlation has a minimum effect in the CO emissions when the 3D model is used, which could be seen in the results shown in Tables 5 and 6. In the 60-kW simulation results (Fig. 11) is also clear that the char correlations do not have a significant effect with the 3D model. For its part, the 1D model shows different concentrations of CO in the lower region of the freeboard but the CO is consumed when the secondary air injection reaches the flame and the overall effect of the char correlation has no effect in the overall boiler behaviour. It can be seen from Figs. 10 and 11 (and also from Tables 5 and 6) that the effect of char correlations is only significant for the half-load boiler operating conditions, when the combustion efficiency is lower due to the low energy release concentration. Therefore, a clear conclusion can be extracted from this results,

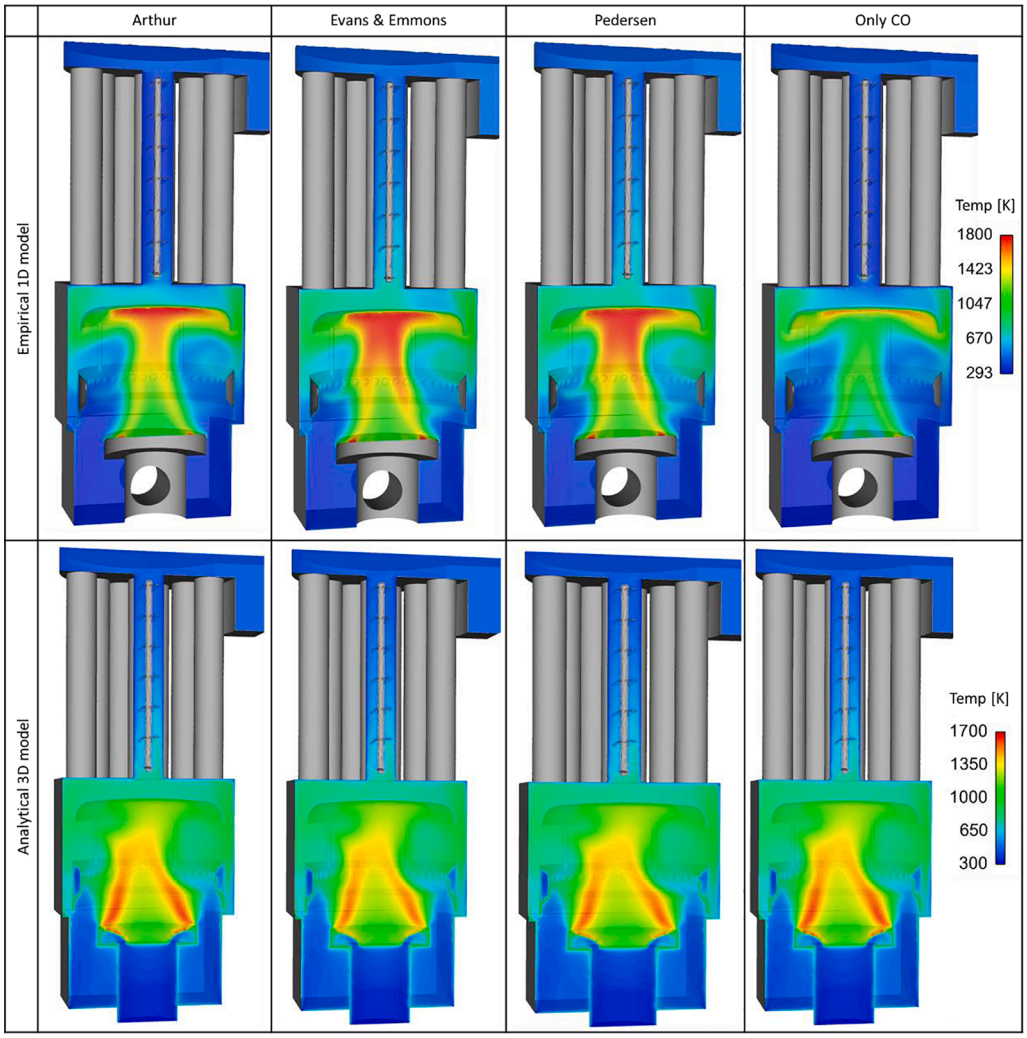

Fig. 12. Contours of gas temperature for the different char oxidation correlations and bed models from the 30-kW test simulation.

the char correlation does not have a significant influence when the combustion conditions are favourable and the boiler efficiency is high. Otherwise, when the conditions do not favour a complete combustion in the freeboard region, the char correlation has an important influence being the Evans & Emmons's and Pedersen's the most advisable ones.

A similar analysis of the combustion efficiency can be performed through the temperature contours. The temperatures in the middle plane of the boiler, for the simulations of the 30-kW test, with the four char oxidation models, are shown in Fig. 12. In this case, the pure-CO-production with the 1D bed model produces a mild combustion in the freeboard and the flame hardly reaches temperatures over 1200 K. This prevents the combustion to be completed and produces a high amount of unburnt species. This is the reason why there are excessive CO and volatile emissions in the flue gases, as shown in Table 5. Therefore, this model is not advisable. The Arthur's correlation also produces high amounts of CO, which implies a lower heat release during the char oxidation due the lower heat of reaction. This produces a lower temperature of the bed that delays the later volatiles combustion. Fig. 12 shows that the highest temperatures (around 1800 K) are appeared when the flame touches the dome in the freeboard. It also shows a quick cooling in the heat exchanger. In this case, the flame quenching is significant with this model and excessive unburnt species can be found in the fumes. The higher temperatures and most voluminous flames are produced with the Evans & Emmons's and the Pedersen's correlations, whose behaviour is very similar in all the simulations. Again, there are no significant differences with the four char correlations when the 3D bed model is used. All the simulations have a similar behaviour, even when the pure CO production is applied. The high temperature and the gas mixing produced in the porous bed activate an early combustion that compensates any differences in the CO/CO_2 ratios of the different char correlations.

The temperature contours of the 60-kW test, shown in Fig. 13, have the same trends as the 30-kW test. Nevertheless, in this case, the high energy supply produces high temperatures in the flame and compensates the delay in combustion of the Arthur's and Pure-CO correlations. This is the main cause because the combustion is complete in all the cases and no unburnt species are found, as we could watch in Table 5.

5. Conclusions

Two CFD fixed bed models of biomass thermal conversion are presented and compared through the simulation of two tests in a domestic boiler operating at a thermal power of 30 and 60 kW. The first model is a 1D empirical method which is solved out of the computational domain. The solution is based on mass and energy balances and the results are exchanged with the CFD domain through a boundary condition that represents the bed top. The second model is an analytical 3D representation that includes the packed bed into the computational domain and locally solves the mass, energy and species balances though UDF and introduces the results of the balances as volumetric sources. Four char oxidation correlations are tested for both bed models to predict different CO/CO_2 production ratios. These correlations are proposed by Arthur,

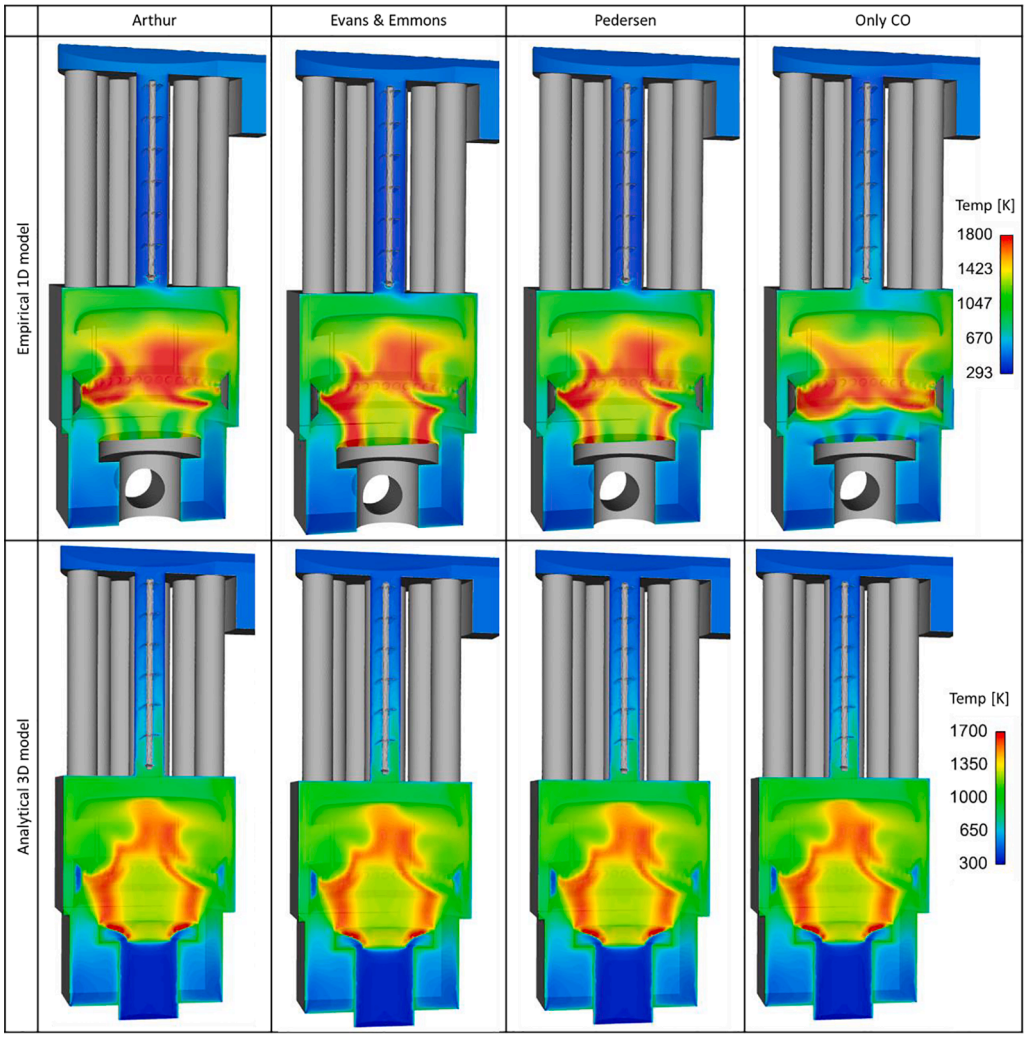

Fig. 13. Contours of gas temperature for the different char oxidation correlations and bed models from the 60-kW test simulation.

Evans & Emmons, Pedersen and the fourth one produces only CO.

Both bed models predict a similar behaviour of the boiler. The 1D empirical model trends to predict a lower heat transferred to water and higher fumes temperatures than the 3D analytical model at the same conditions. Whereas, for the 3D model, the char correlations give virtually the same results. For the 1D model the char correlations have an important effect in the 30 kW test. No significant differences are found in the 60 kW test. The Evans & Emmons's and Pedersen's correlations show a better agreement with the experiments in CO emissions. The Arthur's and especially the pure CO production show excessive CO emissions for the low-power test when the 1D empirical model is used.

In the analysis of combustion variables, the 1D empirical model predicts higher temperatures in the flame core but a lower temperature in the rest of the freeboard volume. It also shows clearly higher concentrations of CO and volatiles in the flame. As the 3D analytical model allows the combustion in the bed region, it advances the combustion in the bed and produces lower temperature gradients and lower combustible species in the freeboard. This fact compensates the differences in the behaviour of the different char oxidation correlations when the 3D analytical model is used. Otherwise, the 1D empirical model suffers a delay in the reactions with the Arthur's correlation and pure-CO production. The effect of this delay is noticeable in the low-power test and produces a longer flame that is insufficient to consume high CO concentrations. In the high-power test, the combustion delay is also visible but the higher energy release allows consuming the CO in the freeboard and, therefore, the different char correlations have not any effect in the overall boiler behaviour.

The 3D model showed a good agreement with experiments and has an acceptable computational cost for some domestic boilers, especially those with low-size packed beds. However, it can be excessive for boilers with large beds or multi-pass heat exchangers. In such cases, the 1D model can be notably more efficient due to the packed bed simplification and the lower number of species required.

CRediT authorship contribution statement

B. Rajh: Conceptualization, Methodology, Investigation, Writing – original draft, Writing – review & editing, Supervision. **M.A. Gómez:** Conceptualization, Methodology, Investigation, Writing – original draft, Writing – review & editing, Supervision. **C. Álvarez-Bermúdez:** Methodology, Investigation, Resources, Supervision. **N. Cid:** Writing – review & editing, Visualization, Supervision. **J.L. Míguez:** Visualization, Resources.

Declaration of Competing Interest

The authors declare that they have no known competing financial interests or personal relationships that could have appeared to influence the work reported in this paper.

Data availability

Data will be made available on request.

Acknowledgements

The authors are grateful for financial support from the Slovenian Research Agency (Research Core Funding No. P2-0424) and the Ministry of Science and Innovation of Spain (project PID2021-126569OB-I00).

Funding for open access charge: Universidade de Vigo/CISUG

References

[1] Scarlat N, Dallemand J, Monforti-Ferrario F, Nita V. The role of biomass and bioenergy in a future bioeconomy Policies and facts. Environ Dev 2015;15:3–34.
[2] Popp J, Kovács S, Oláh J, Divéki Z, Balázs E. Bioeconomy: Biomass and biomass-based energy supply and demand. New Biotechnol 2021;60:76–84.
[3] J. Islas, F. Manzini, O. Masera, V. Vargas, Solid biomass to heat and power, in: Anonymous The Role of Bioenergy in the Emerging Bioeconomy: Resources, Technologies, Sustainability and Policy, , 2018, pp. 145-177.
[4] The European Green Deal, https://ec.europa.eu/info/strategy/priorities-2019-2024/european-green-deal_en,.
[5] Fit to 55 package, https://www.consilium.europa.eu/en/policies/green-deal/fit-for-55-the-eu-plan-for-a-green-transition/,.
[6] Carvalho L, Wopienka E, Pointner C, Lundgren J, Verma VK, Haslinger W, et al. Performance of a pellet boiler fired with agricultural fuels. Appl Energy 2013;104:286–96.
[7] Büchner D, Schraube C, Carlon E, von Sonntag J, Schwarz M, Verma VK, et al. Survey of modern pellet boilers in Austria and Germany - System design and customer satisfaction of residential installations. Appl Energy 2015;160:390–403.
[8] Míguez JL, Morán JC, Granada E, Porteiro J. Review of technology in small-scale biomass combustion systems in the European market. Renewable Sustainable Energy Rev 2012;16(6):3867–75.
[9] Jach-Nocoń M, Pełka G, Luboń W, Mirowski T, Nocoń A, Pachytel P. An assessment of the efficiency and emissions of a pellet boiler combusting multiple pellet types. Energies 2021;14(15):4465.
[10] Álvarez-Bermúdez C, Chapela S, Varela LG, Gómez MÁ. Cfd simulation of an internally cooled biomass fixed-bed combustion plant. Resources 2021;10(8):77.
[11] Anca-Couce A, Hochenauer C, Scharler R. Bioenergy technologies, uses, market and future trends with Austria as a case study. Renewable Sustainable Energy Rev 2021;135:110237.
[12] Zadravec T, Rajh B, Kokalj F, Samec N. Influence of air staging strategies on flue gas sensible heat losses and gaseous emissions of a wood pellet boiler: An experimental study. Renew Energy 2021;178:532–48.
[13] Liu H, Chaney J, Li J, Sun C. Control of NOx emissions of a domestic/small-scale biomass pellet boiler by air staging. Fuel 2013;103:792–8.
[14] Stanisławski R, Junga R, Nitsche M. Reduction of the CO emission from wood pellet small-scale boiler using model-based control. Energy 2022;243:123009.
[15] Brunner T, Obernberger I, Scharler R. Primary measures for low-emission residential wood combustion - Comparison of old with optimised modern systems. In: Proceedings of the 17th European Biomass Conference & Exhibition; 2009. p. 1319–28.
[16] Bianco V, Szubel M, Matras B, Filipowicz M, Papis K, Podlasek S. CFD analysis and design optimization of an air manifold for a biomass boiler. Renew Energy 2021;163:2018–28.
[17] Chapela S, Porteiro J, Garabatos M, Patiño D, Gómez MA, Míguez JL. CFD study of fouling phenomena in small-scale biomass boilers: Experimental validation with two different boilers. Renew Energy 2019;140:552–62.
[18] Chaney J, Liu H, Li J. An overview of CFD modelling of small-scale fixed-bed biomass pellet boilers with preliminary results from a simplified approach. Energy Convers Manage 2012;63:149–56.
[19] Yin C, Rosendahl LA, Kær SK. Grate-firing of biomass for heat and power production. Prog Energy Combust Sci 2008;34(6):725–54.
[20] Rajh B, Yin C, Samec N, Hriberšek M, Zadravec M. Advanced modelling and testing of a 13 MWth waste wood-fired grate boiler with recycled flue gas. Energy Convers Manage 2016;125:230–41.
[21] Zadravec T, Rajh B, Kokalj F, Samec N. CFD modelling of air staged combustion in a wood pellet boiler using the coupled modelling approach. Therm Sci Eng Prog 2020;20:100715.
[22] Buchmayr M, Gruber J, Hargassner M, Hochenauer C. A computationally inexpensive CFD approach for small-scale biomass burners equipped with enhanced air staging. Energy Convers Manage 2016;115:32–42.
[23] Scharler R, Gruber T, Ehrenhöfer A, Kelz J, Bardar RM, Bauer T, et al. Transient CFD simulation of wood log combustion in stoves. Renew Energy 2020;145:651–62.
[24] Buss F, Wirtz S, Scherer V. Simulation of a reacting agitated bed of straw pellets by a resolved coupled DEM/CFD method using a blocked-off approach. Int J Therm Sci 2020;152:106332.
[25] Wiese J, Wissing F, Höhner D, Wirtz S, Scherer V, Ley U, et al. DEM/CFD modeling of the fuel conversion in a pellet stove. Fuel Process Technol 2016;152:223–39.
[26] Somwangthanaroj S, Fukuda S. CFD modeling of biomass grate combustion using a steady-state discrete particle model (DPM) approach. Renew Energy 2020;148:363–73.
[27] Gómez MA, Porteiro J, Patiño D, Míguez JL. Eulerian CFD modelling for biomass combustion. Transient simulation of an underfeed pellet boiler. Energy Convers Manage 2015;101:666–80.
[28] Hermansson S, Thunman H. CFD modelling of bed shrinkage and channelling in fixed-bed combustion. Combust Flame 2011;158(5):988–99.
[29] Collazo J, Porteiro J, Patiño D, Granada E. Numerical modeling of the combustion of densified wood under fixed-bed conditions. Fuel 2012;93:149–59.
[30] Gómez MA, Martín R, Chapela S, Porteiro J. Steady CFD combustion modeling for biomass boilers: An application to the study of the exhaust gas recirculation performance. Energy Convers Manage 2019;179:91–103.
[31] Li J, Paul MC, Younger PL, Watson I, Hossain M, Welch S. Characterization of biomass combustion at high temperatures based on an upgraded single particle model. Appl Energy 2015;156:749–55.
[32] Zadravec T, Yin C, Kokalj F, Samec N, Rajh B. The impacts of different profiles of the grate inlet conditions on freeboard CFD in a waste wood-fired grate boiler. Appl Energy 2020;268:115055.
[33] Costa M, Massarotti N, Indrizzi V, Rajh B, Yin C, Samec N. Engineering bed models for solid fuel conversion process in grate-fired boilers. Energy 2014;77:244–53.
[34] Rajh B, Yin C, Samec N, Hriberšek M, Kokalj F, Zadravec M. Advanced CFD modelling of air and recycled flue gas staging in a waste wood-fired grate boiler for higher combustion efficiency and greater environmental benefits. J Environ Manage 2018;218:200–8.
[35] Fu WB, Zhang BL, Zheng SM. A relationship between the kinetic parameters of char combustion and the coal's properties. Combust Flame 1997;109(4):587–98.
[36] Phillips R, Vastola FJ, Walker PL. Factors affecting the product ratio of the carbon-oxygen reaction-II Reaction temperature. Carbon 1970;8(2):205–10.
[37] Geier M, Shaddix CR, Holzleithner F. A mechanistic char oxidation model consistent with observed CO 2/CO production ratios. Proc Combust Inst 2013;34(2):2411–8.
[38] Mehrabian R, Zahirovic S, Scharler R, Obernberger I, Kleditzsch S, Wirtz S, et al. A CFD model for thermal conversion of thermally thick biomass particles. Fuel Process Technol 2012;95:96–108.
[39] Anca-Couce A, Sommersacher P, Shiehnejadhesar A, Mehrabian R, Hochenauer C, Scharler R. CO/CO2 ratio in biomass char oxidation. Energy Procedia 2017;120:238–45.
[40] Westbrook CK, Dryer FL. Prediction of laminar flame properties of methanol-air mixtures. Combust Flame 1980;37:171–92.
[41] Arthur JR. Reactions between carbon and oxygen. Trans Faraday Soc 1951;47:164–78.
[42] Evans DD, Emmons HW. Combustion of wood charcoal. Fire Saf J 1977;1(1):57–66.
[43] K. Pedersen, No title, The Product Ratio of CO/CO_2 in the Oxidation of Biomass Char. (2003).
[44] Ergun S. Fluid flow through packed columns. Chem Eng Prog 1952;48:89–94.
[45] Gómez MA, Porteiro J, Patiño D, Míguez JL. CFD modelling of thermal conversion and packed bed compaction in biomass combustion. Fuel 2014;117:716–32.
[46] Gómez MA, Patiño D, Comesaña R, Porteiro J, Álvarez Feijoo MA, Míguez JL. CFD simulation of a solar radiation absorber. Int J Heat Mass Transf 2013;57(1):231–40.
[47] Wakao N, Kaguei S, Funazkri T. Effect of fluid dispersion coefficients on particle-to-fluid heat transfer coefficients in packed beds. Correlation of nusselt numbers. Chem Eng Sci 1979;34(3):325–36.
[48] Wagenaar BM, Prins W, van Swaaij WPM. Flash pyrolysis kinetics of pine wood. Fuel Process Technol 1993;36(1-3):291–8.
[49] Bryden KM, Ragland KW. Numerical modeling of a deep, fixed bed combustor. Energy Fuels 1996;10(2):269–75.
[50] Gómez MA, Porteiro J, Chapela S, Míguez JL. An Eulerian model for the simulation of the thermal conversion of a single large biomass particle. Fuel 2018;220:671–81.
[51] Thunman H, Niklasson F, Johnsson F, Leckner Bo. Composition of volatile gases and thermochemical properties of wood for modeling of fixed or fluidized beds. Energy Fuels 2001;15(6):1488–97.
[52] Neves D, Thunman H, Matos A, Tarelho L, Gómez-Barea A. Characterization and prediction of biomass pyrolysis products. Prog Energy Combust Sci 2011;37(5):611–30.
[53] Anca-Couce A. Reaction mechanisms and multi-scale modelling of lignocellulosic biomass pyrolysis. Prog Energy Combust Sci 2016;53:41–79.